Pergamon

Geochimica et Cosmochimica Acta, Vol. 67, No. 3, pp. 543–555, 2003

0016-7037/03 $22.00 + .00

PII S0016-7037(02)01117-1

Diopside-bearing EL6 EET 90102: Insights from rare earth element distributions

CHRISTINE FLOSS,[1,*] ROBERT A. FOGEL,[2] YANGTING LIN,[3] and MAKOTO KIMURA[4]

[1]Laboratory for Space Sciences and the Department of Earth and Planetary Sciences, Washington University, St. Louis, MO 63130, USA
[2]Department of Earth and Planetary Sciences, American Museum of Natural History, New York, NY 10024, USA
[3]Guangzhou Institute of Geochemistry, Chinese Academy of Sciences, Guangzhou 510640, China
[4]Astrophysics and Planetary Science, Faculty of Science, Ibaraki University, Mito 310-8512, Japan

(*Received December* 17, 2001; *accepted in revised form July* 25, 2002)

Abstract—EET 90102 is the first known diopside-bearing EL6 chondrite. Diopside occurs in most aubrites and is occasionally found as rare small grains in unequilibrated enstatite chondrites, but is unknown from equilibrated enstatite chondrites. We have carried out a study of the rare earth element (REE) distributions in EET 90102, with a specific emphasis on diopside, in order to better understand its origin in this meteorite. We also present data for Ca-rich pyroxenes from two unequilibrated (EH3) enstatite chondrites for comparison.

Our data show that diopside and other silicates in EET 90102 exhibit volatility-related anomalies indicative of formation under highly reducing conditions. Such anomalies have not previously been observed in EL6 chondrites, although they are common in unequilibrated enstatite chondrites. Diopside in EET 90102 probably formed by metamorphic equilibration of enstatite and oldhamite. The REE compositions of some grains, in particular the presence of positive Yb anomalies, indicate that they inherited their REE characteristics largely from CaS. Other grains have REE patterns that are more consistent with a derivation of diopside primarily from enstatite.

In contrast to other EL6 chondrites, which experienced slow cooling, EET 90102 was quenched from high metamorphic temperatures. Thus, there may have been insufficient time to completely homogenize diopside REE compositions.

The presence of diopside in EET 90102 simplifies one outstanding problem of aubrite formation. Melting of a diopside-bearing enstatite chondrite protolith provides a source for the abundant diopside in aubrites without requiring the oxidation of oldhamite, as suggested by previous research.

1. INTRODUCTION

The enstatite meteorites, comprising the EH and EL chondrites and the achondritic aubrites, consist of highly reduced mineral assemblages and must have formed in a unique region of the solar system (Keil, 1968, 1989; Watters and Prinz, 1979). Dominated by nearly Fe-free enstatite (FeO generally less than 1.0 wt.%; Keil, 1968), they also contain a host of unusual minerals that are unknown or rare in other terrestrial or extraterrestrial rocks. Typically, lithophile elements form sulfide phases such as oldhamite (CaS), niningerite (MgS), and alabandite (MnS). Nitrogen-rich minerals such as sinoite (Si_2N_2O) and osbornite (TiN) are also present. Other silicate phases found in the enstatite meteorites include albite, silica, forsterite, and diopside. Of these, diopside is of particular interest because it is relatively abundant in aubrites (Watters and Prinz, 1979) and is occasionally found as small rare grains in unequilibrated (E3–4) enstatite chondrites (Rambaldi et al., 1983; Grossman et al., 1985; Kitamura et al., 1987; Lin et al., 1991; Kimura et al., 2000). Before its discovery in EET 90102 (Fogel, 1995), however, diopside had not been reported in equilibrated (E5–6) enstatite chondrites. This absence was all the more unusual because enstatite CaO contents are high in EL6 chondrites and might be expected to result in the formation of stable diopside during metamorphic equilibration (Fogel et al., 1989). However, Fogel (1997a) noted that bulk compositions of nominal EL6 chondrites lie in the enstatite–oldhamite–alabandite stability field, whereas the bulk composition of EET 90102 lies in the enstatite–diopside–oldhamite–alabandite stability field.

The petrology and mineral chemistry of EET 90102 were described in detail by Fogel (1997a) who noted that, despite slight compositional differences, this meteorite is closely related to other EL6 chondrites. In this study we investigated the rare earth element (REE) distributions of EET 90102 to gain additional insights into its petrogenesis. In particular we were interested in gaining a better understanding of the origin of diopside in this meteorite. Because comparable trace element data for diopside from unequilibrated enstatite chondrites do not yet exist, we also measured the REE abundances of a number of diopside grains from two EH3 chondrites, Qingzhen and Sahara 97159. Preliminary results were reported by Floss and Fogel (2001) and Floss et al. (2001).

2. EXPERIMENTAL

The thin section of EET 90102 examined here is ,9, the same one studied by Fogel (1997a). In addition, diopside grains were located and analyzed from the EH3 chondrites, Qingzhen (QZ2–4 from the Guangzhou Institute of Geochemistry) and Sahara 97159 (section ,1 from the Guangzhou Institute of Geochemistry). Major and minor element compositions (Table 1) were determined using a JEOL 733 electron microprobe with an accelerating voltage of 15 kV and a beam current of 10 nA. Detection limits are (1σ in wt.%): Na_2O: 0.04; K_2O: 0.04; TiO_2: 0.07; Cr_2O_3: 0.07; MnO: 0.12. After initial documentation and characterization, using a JEOL 840a scanning electron microscope, the REE and other trace elements were measured using a modified Cameca IMS-3f ion microprobe, according to methods described by Zinner and Crozaz (1986a). Secondary ions were sputtered from the sample sur-

* Author to whom correspondence should be addressed (floss@wuphys.wustl.edu).

Table 1. Major element concentrations (in wt.%) for EET 90102 silicates and EH3 diopsides.

	EET 90102 silicates[a]			Sahara 97159 diopside[b]						Qingzhen diopside
	albite	enstatite	diopside	97-07	97-29	97-46	97-53	97-58	97-59	QZ2-4-01
SiO_2	66.44	59.67	55.85	50.70	50.16	52.31	42.98	52.68	46.24	49.93
TiO_2	b.d.	b.d.	b.d.	1.02	0.41	0.51	1.40	0.36	1.34	1.43
Al_2O_3	20.23	0.10	0.31	3.07	10.78	2.46	19.10	1.98	13.20	9.63
Cr_2O_3		b.d.	b.d.	0.68	0.59	0.73	0.42	1.73	1.37	0.30
FeO	0.36	0.28	0.28	7.10	0.32	12.05	3.32	4.65	1.48	0.29
MnO	b.d.	b.d.	b.d.	0.34	0.18	0.22	b.d.	0.68	0.13	b.d.
MgO	b.d.	39.72	19.44	18.26	18.70	22.65	9.35	19.88	15.20	18.47
CaO	2.11	0.74	24.30	16.43	18.14	8.55	2.44	15.57	20.47	20.76
Na_2O	9.66	b.d.	0.14	0.01	0.13	0.30	b.d.	0.39	b.d.	0.13
K_2O	0.97			b.d.	b.d.	b.d.	b.d.	b.d.	b.d.	b.d.
Total	99.88	100.49	100.32	97.61	99.41	99.78	100.01	97.92	99.43	100.94
Si	11.726	1.991	1.998	1.899	1.785	1.913	1.571	1.944	1.677	
Ti				0.029	0.011	0.014	0.039	0.010	0.037	
Al	4.207	0.004	0.013	0.136	0.452	0.106	0.823	0.086	0.564	
Cr				0.020	0.017	0.021	0.012	0.051	0.039	
Fe	0.054	0.008	0.009	0.222	0.010	0.369	0.102	0.144	0.045	
Mn				0.011	0.005	0.007		0.021	0.004	
Mg		1.976	1.037	1.019	0.992	1.235	0.509	1.093	0.822	
Ca	0.400	0.026	0.931	0.659	0.692	0.335	0.918	0.616	0.796	
Na	3.305		0.010	0.001	0.009	0.021		0.028		
K	0.217									
Total	19.909	4.005	3.998	3.995	3.973	4.020	3.974	3.992	3.984	

[a] Data from Fogel (1997a): plagioclase stoichiometry based on 32 oxygens, others on 6 oxygens.
[b] Stoichiometry based on 12 oxygens.
b.d. = below detection.

faces and collected at low mass resolution, using energy filtering to remove complex molecular interferences. Simple molecular interferences (e.g., SiO^+) are not removed by this method and are corrected for using an analysis program developed to deconvolve major molecular interferences for the elements K-Ca-Sc-Ti, Rb-Sr-Y-Zr, and Ba-REEs (Alexander, 1994; Hsu, 1995). Measurements were made using O^- primary beams of ~0.5 to 5 nA, depending on the size of the grain and expected REE abundances. Beam currents were somewhat higher (~10 nA) for analyses of relict chondrule fragments to obtain larger sputter areas (50 to 75 μm) and, thus, more representative analyses.

The sensitivity factors used for the REE in the silicates are those of Zinner and Crozaz (1986b), except for those in plagioclase, which are from Floss and Jolliff (1998). REE concentrations were determined by normalization to the reference element, Si. SiO_2 concentrations for EET 90102 silicates (Table 1) are averages given in Fogel (1997a); relict chondrule analyses are normalized to nominal SiO_2 concentrations of 50.0 wt.% because bulk major element compositions for the chondrules are not known. SiO_2 concentrations for EH3 diopsides were determined by electron microprobe analyses of the specific grains analyzed (Table 1). The sensitivity factors used for the analysis of the oldhamite grain in EET 90102 are from Fahey et al. (1995). Because the oldhamite grain is moderately weathered, and it is not clear how much Ca (the reference element) or REE were lost, absolute REE concentrations cannot be determined. In calculating REE concentrations for this grain, we have assumed that Ca and the REE were lost to the same extent and used the same reference Ca concentration as for unweathered oldhamite (53.0 wt.%). The REE abundances shown in Figure 1 reflect this normalization procedure. See Floss and Crozaz (1993) for a more detailed discussion of oldhamite weathering and its effect on REE abundances.

Analysis spots were carefully chosen before measurements to avoid cracks and inclusions and were examined afterwards to check for contamination in the third dimension. In addition, masses diagnostic of potential contaminating phases were continuously monitored during all analyses. REE abundances in the figures are normalized to the CI chondrite abundances of Anders and Grevesse (1989).

3. RESULTS

3.1. EET 90102

EET 90102 is dominated by enstatite and also contains albite, kamacite, and sulfide phases in proportions similar to those of other EL6 chondrites (Fogel, 1997a). In addition, it contains ~1 vol.% diopside. Although it has a recrystallized texture typical of equilibrated enstatite chondrites, it also contains a number of moderately well-defined relict chondrule fragments. We measured the REE in the three major silicate phases (enstatite, albite, and diopside) and in a number of the

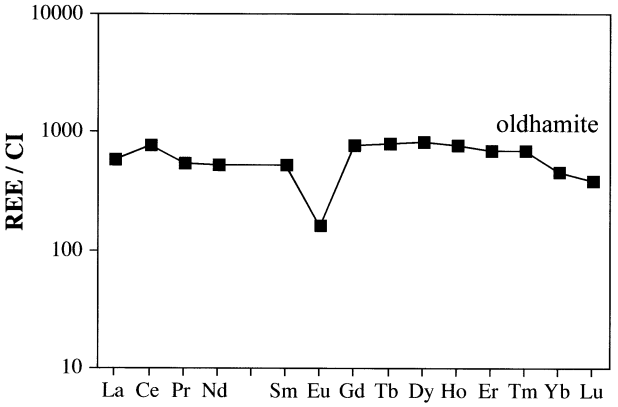

Fig. 1. CI chondrite-normalized REE pattern for a weathered oldhamite grain from EET 90102. The REE abundances shown assume equal loss of Ca and the REE during weathering.

Table 2. REE concentrations (in ppb) in EET 90102 silicates[a].

		Diopside						
	Albite	#1	#2	#3	#4	#5	#6	Enstatite ave. of 9
Anomaly		−Sm?, +Yb	−Eu	+Yb	−Sm?, +Yb	−Sm?	−Eu	
La	190 ± 30	44 ± 8	110 ± 20	54 ± 10	65 ± 9	82 ± 11	91 ± 31	b.d.
Ce	34 ± 11	150 ± 20	300 ± 40	110 ± 20	140 ± 20	240 ± 20	250 ± 90	b.d.
Pr	3.5 ± 4.1	21 ± 6	46 ± 9	22 ± 7	22 ± 6	39 ± 8	36 ± 5	b.d.
Nd	0.9 ± 8.1	140 ± 20	150 ± 30	98 ± 18	100 ± 15	200 ± 20	190 ± 55	b.d.
Sm	b.d.	25 ± 15	130 ± 30	29 ± 18	16 ± 14	35 ± 16	55 ± 4	0.2 ± 0.2
Eu	310 ± 50	26 ± 7	21 ± 6	15 ± 6	15 ± 5	10 ± 5	9.2 ± 7.5	b.d.
Gd	b.d.	91 ± 24	240 ± 40	84 ± 25	52 ± 18	100 ± 30	91 ± 61	3.9 ± 2.2
Tb	b.d.	15 ± 6	44 ± 11	15 ± 6	11 ± 5	18 ± 6	15 ± 3	2.1 ± 1.5
Dy	b.d.	150 ± 20	310 ± 30	140 ± 20	130 ± 20	160 ± 20	130 ± 50	17 ± 9
Ho	b.d.	28 ± 7	94 ± 14	26 ± 8	37 ± 7	73 ± 11	28 ± 14	6.4 ± 2.8
Er	b.d.	97 ± 15	250 ± 30	100 ± 20	110 ± 20	220 ± 20	140 ± 10	27 ± 10
Tm	b.d.	19 ± 6	27 ± 9	13 ± 6	13 ± 5	16 ± 6	17 ± 7	6.9 ± 2.4
Yb	b.d.	260 ± 40	270 ± 50	280 ± 50	280 ± 40	270 ± 40	170 ± 10	59 ± 10
Lu	b.d.	22 ± 8	32 ± 11	17 ± 8	14 ± 8	47 ± 11	32 ± 3	12 ± 4
Sm/Sm*		0.45			0.46	0.50		
Eu/Eu*			0.37				0.39	
Yb/Yb*		1.87		2.76	3.20			

[a] Errors are 1σ standard deviation.

chondrule fragments. We also analyzed one small weathered oldhamite (CaS) grain found in a chondrule fragment. The REE data are presented in Tables 2–3 and Figures 1–4, and are discussed in detail below.

3.1.1. Albite and Enstatite

REE abundances are generally quite low in silicates from enstatite meteorites (Floss et al., 1990; Floss and Crozaz, 1993; Hsu and Crozaz, 1998; Hsu, 1998), and those from EET 90102 are no exception. The single albite we analyzed is an individual grain surrounded by metal and troilite on three sides. Only the light REE (LREE) La–Nd, and Eu have concentrations above detection limits (Table 2, Fig. 2). Enstatite REE abundances are also low, with only Sm–Lu above detection. The nine enstatite grains that we measured occur as individual grains in the matrix of EET 90102 and are surrounded by metal, troilite, and other enstatite grains. All grains have similar REE abundances (Table 2) and a REE pattern that is most similar to enstatite pattern III of Hsu and Crozaz (1998); the pattern contains no anomalies other than an implied (because abundances are below detection limits) negative Eu anomaly (Fig. 2).

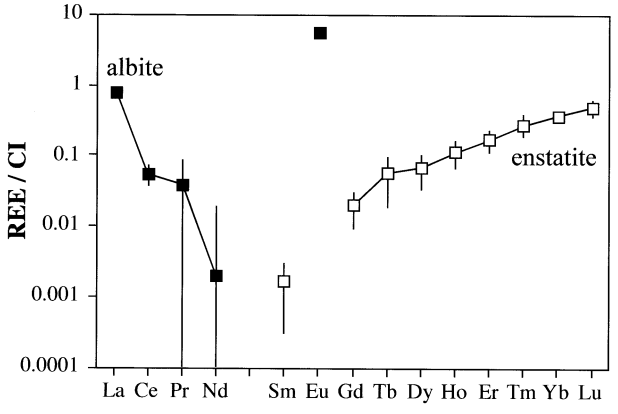

Fig. 2. CI chondrite-normalized REE patterns for albite and enstatite from EET 90102. The enstatite pattern is the average of nine analyses. Elements not shown are below detection limits.

3.1.2. Diopside

We measured six distinct diopside grains from EET 90102 (Table 2, Fig. 3). Five of these occur as individual grains associated with enstatite or metal in the matrix of EET 90102. The other grain, diopside #1, is part of a larger diopside–plagioclase aggregate. The patterns are flat to somewhat heavy REE (HREE)-enriched (chondrite-normalized Lu/La ratios are $\leq$5.5) and have abundances between 0.1 and 2 $\times$ CI. Three of the grains, #1, #3, and #4, have positive Yb anomalies (Fig. 3); these are the first reported occurrences of positive Yb anomalies in diopside from enstatite meteorites. Grains #1, #4, and #5 also show slight hints of negative Sm anomalies, although the errors are large (Table 2). Finally, one diopside (#5) appears to be somewhat depleted in Tm (Fig. 3).

Floss et al. (2001) reported the analysis of a diopside grain in EET 90102 with elevated REE abundances ($\sim$10 $\times$ CI) and a pattern similar in shape to that of the single oldhamite grain measured in this sample (see below and Fig. 1). Although the count rates of S masses monitored to check for CaS contamination did not indicate the presence of oldhamite in this analysis, a repeat measurement of the same spot resulted in even higher abundances of the REE and somewhat higher Ca contents. A third measurement of the diopside grain, in a spot immediately adjacent to the original sputter hole, produced a somewhat different REE pattern with distinctly lower REE abundances (diopside #6 in Fig. 3). It is likely, therefore, that oldhamite contamination is in fact responsible for the elevated abundances and REE pattern originally observed. This was probably a highly weathered grain that had lost much of its S. Oldhamite is known to weather into portlandite, vaterite, cal-

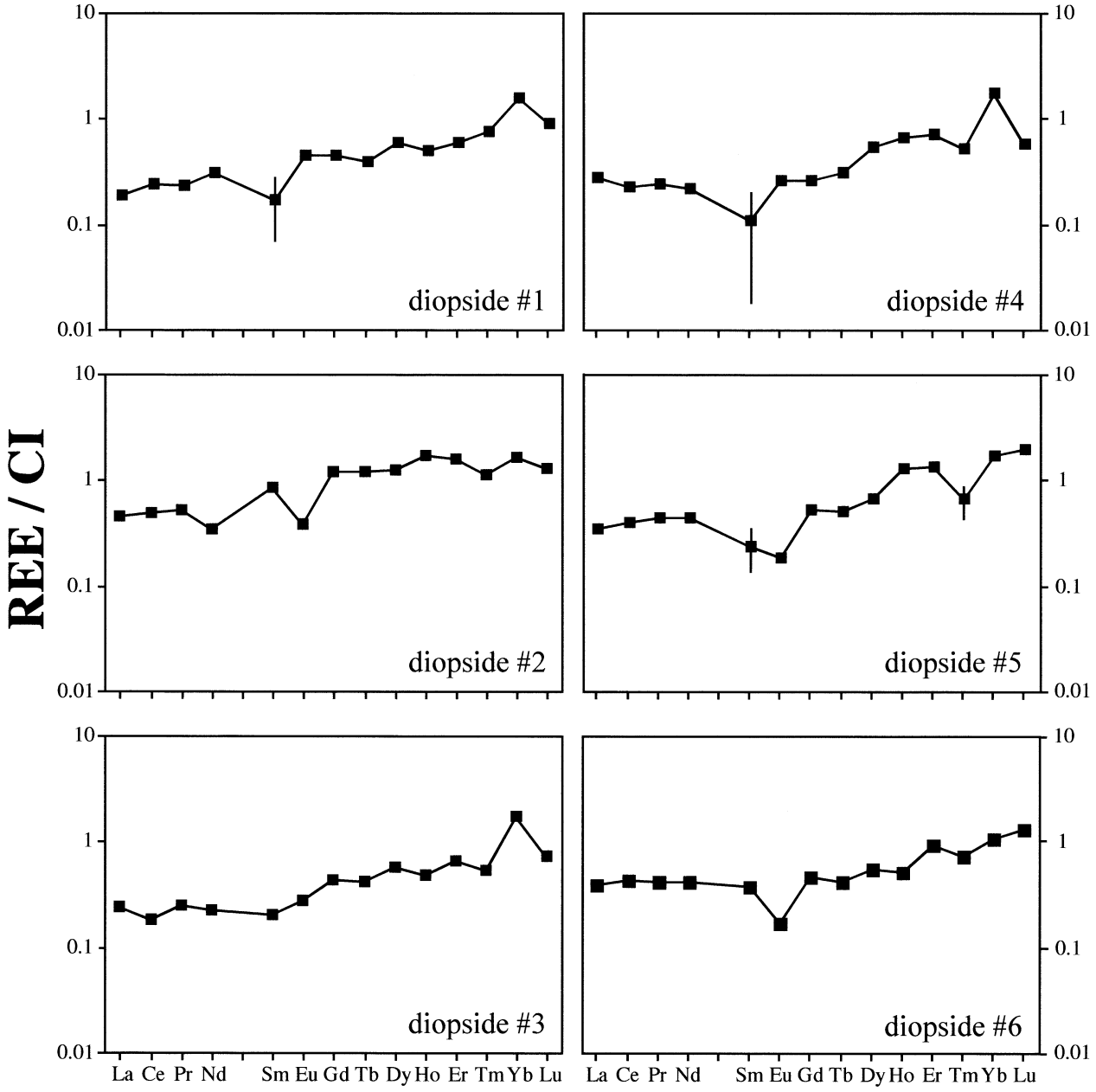

Fig. 3. CI chondrite-normalized REE patterns for diopside from EET 90102. Error bars are shown only for some elements (e.g., Sm, Tm).

cite, and bassanite, all of which are depleted in S relative to CaS (Okada et al., 1981).

3.1.3. Relict Chondrules

REE patterns of the eight relict chondrule fragments analyzed are reported in Table 3 and portrayed graphically in Figure 4. Chondrule #1 is described by Fogel (1997a) as a remnant radial pyroxene (enstatite) chondrule containing long stringers of thin diopside crystals; albite, metal, and troilite are also present (see Fig. 2d of Fogel, 1997a). Most of the other chondrule fragments measured here are also fine-grained radial or barred pyroxene chondrules with varying abundances of these minerals. One chondrule fragment (#4), however, has a fine-grained granulitic texture; this is the same chondrule in which the oldhamite grain, discussed below, occurs. The chondrules range in size from 200 to 900 μm. Three of them (#1, #4, and #5) have more or less flat REE patterns with abundances between 0.2 and 1 $\times$ CI; chondrule #4 also has a small positive Eu anomaly. Two chondrules (#6 and #8) have slightly to moderately V-shaped patterns (e.g., enrichments of both LREE and HREE) with large positive Eu anomalies. Finally, three chondrules (#2, #3, and #7) have HREE-enriched patterns with evidence of negative Sm anomalies. Although the errors on the Sm values are large (Table 3, Fig. 4), the very low count rates obtained consistently throughout these measurements for this element sug-

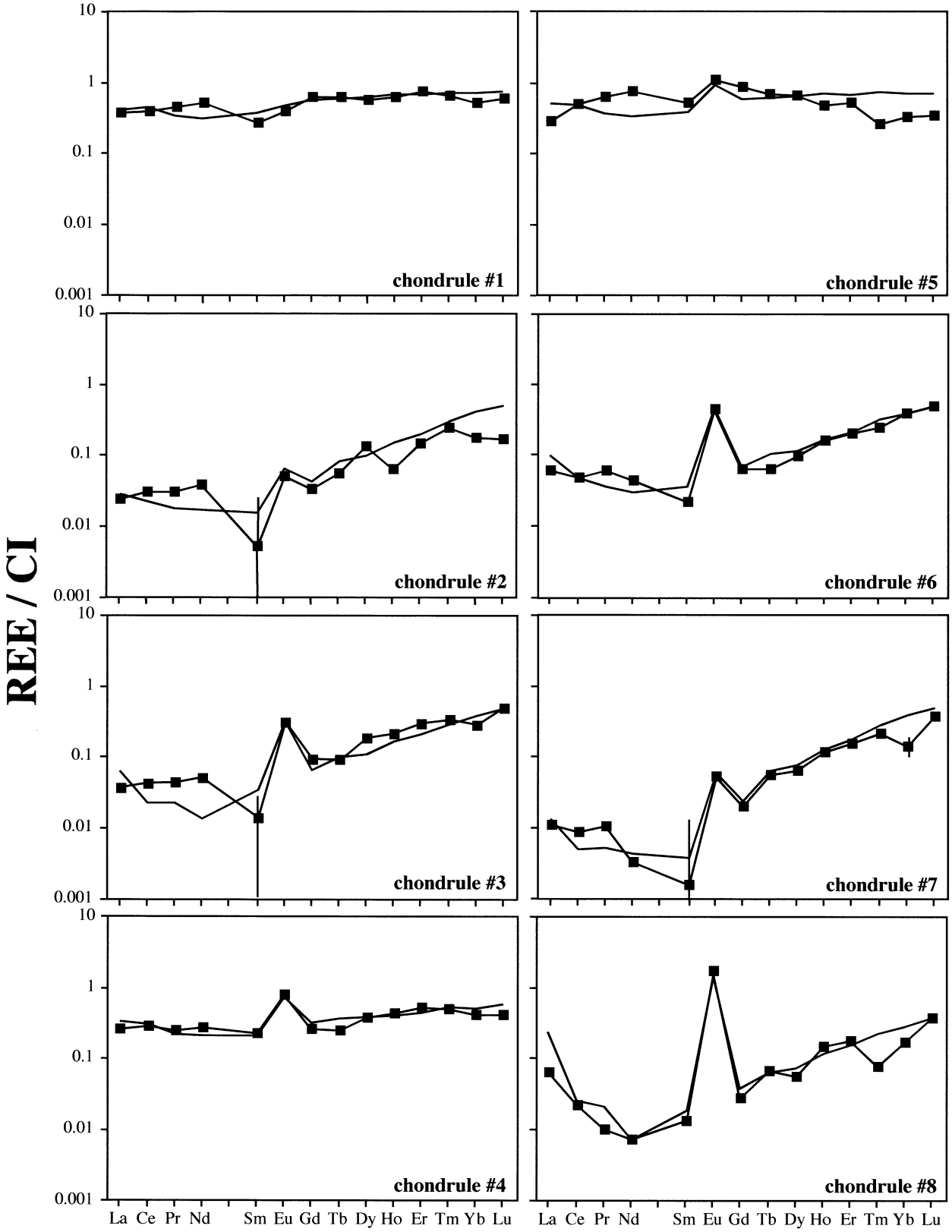

Fig. 4. CI chondrite-normalized REE patterns for relict chondrule fragments from EET 90102. Filled squares show the measured patterns for the chondrules; lines show the results of calculations to reproduce the chondrule compositions from EET 90102 mineral compositions. Error bars are shown only for some elements (e.g., Sm).

Table 3. REE concentrations (in ppb) in EET 90102 relict chondrules[a].

	Relict chondrules							
	#1	#2	#3	#4	#5	#6	#7	#8
Anomaly		−Sm	−Sm, +Eu	+Eu		+Eu	−Sm, +Eu, −Yb	+Eu
La	86 ± 14	5.6 ± 1.6	8.8 ± 1.3	61 ± 10	68 ± 7	14.2 ± 1.3	2.6 ± 1.1	15 ± 2
Ce	240 ± 30	18 ± 3	26 ± 2	170 ± 20	290 ± 20	30 ± 3	5.4 ± 1.8	13 ± 3
Pr	40 ± 7	2.8 ± 1.2	4.0 ± 0.9	22 ± 3	56 ± 6	5.6 ± 0.8	0.9 ± 0.7	0.9 ± 0.7
Nd	230 ± 20	17 ± 4	24 ± 3	120 ± 10	330 ± 20	20 ± 2	1.5 ± 1.4	3.4 ± 2.3
Sm	40 ± 12	0.8 ± 3.5	2.0 ± 2.2	33 ± 8	76 ± 14	3.2 ± 1.8	0.2 ± 1.6	1.9 ± 3.3
Eu	22 ± 5	2.9 ± 1.4	17 ± 3	43 ± 6	60 ± 8	25 ± 4	3.0 ± 1.2	96 ± 13
Gd	130 ± 20	6.6 ± 4.7	18 ± 4	50 ± 10	170 ± 30	13 ± 3	4.0 ± 2.3	5.4 ± 2.5
Tb	23 ± 6	2.1 ± 1.3	3.4 ± 0.9	8.8 ± 2.2	24 ± 5	2.3 ± 0.6	2.0 ± 1.0	2.5 ± 1.1
Dy	140 ± 20	33 ± 5	45 ± 4	92 ± 8	160 ± 10	24 ± 2	15 ± 3	13 ± 3
Ho	34 ± 5	3.6 ± 1.5	12 ± 2	24 ± 3	26 ± 4	8.8 ± 1.1	6.4 ± 1.6	8.3 ± 2.0
Er	120 ± 10	23 ± 4	48 ± 4	82 ± 7	84 ± 10	33 ± 3	25 ± 4	29 ± 5
Tm	16 ± 4	6.0 ± 1.9	8.2 ± 1.4	12 ± 3	6.3 ± 2.6	6.0 ± 1.1	5.2 ± 1.5	1.9 ± 2.8
Yb	84 ± 18	28 ± 9	46 ± 7	67 ± 11	54 ± 15	63 ± 7	23 ± 7	28 ± 8
Lu	14 ± 5	4.1 ± 2.1	12 ± 2	10 ± 3	8.3 ± 3.8	12 ± 2	9.2 ± 2.3	9.0 ± 2.6
Sm/Sm*		0.15	0.19				0.05	
Eu/Eu*			2.58	3.14		10.2	2.01	84
Yb/Yb*							0.48	

[a] Errors are 1σ standard deviation.

gest that the depletions are, in fact, real. Chondrules #3 and #7 also have small to moderate positive Eu anomalies and chondrule #7 has a negative Yb anomaly.

3.1.4. Oldhamite

Although much of the oldhamite originally present in EET 90102 appears to have been weathered out (Fogel, 1997a), we did find one moderately weathered area large enough for ion microprobe analysis. The grain occurs in the fine-grained granulitic chondrule fragment (#4) mentioned above. Several studies have shown that weathering of oldhamite does not substantially alter its REE pattern. Although leaching experiments (Shima and Honda, 1967; Lodders et al., 1993) suggest that Ca and Eu dissolve in water, Lodders et al. (1993) noted that the other REE require more acidic solvents for dissolution. Furthermore, Floss and Crozaz (1993) and Wheelock et al. (1994) showed that weathered portions of oldhamite grains have the same REE pattern shapes (including the relative magnitudes of Eu anomalies) as unweathered regions. Thus, although weathering may occasionally result in some depletion of Eu, the REE are generally not fractionated by this process and, therefore, REE *patterns* (but not abundances) are representative of the original oldhamite grain. The REE pattern for the oldhamite grain analyzed here is shown in Figure 1. It is essentially flat with a negative Eu anomaly, similar to the REE pattern observed in oldhamite from other EL6 chondrites (Floss and Crozaz, 1993; Crozaz and Lundberg, 1995). However, the REE abundances shown in Figure 1 are on the order of 400−800 × CI, clearly indicating that Ca was lost preferentially to the REE. Unweathered oldhamite grains from other EL6 chondrites have REE concentrations that are approximately an order of magnitude lower than this (Floss and Crozaz, 1993; Crozaz and Lundberg, 1995).

3.2. EH3 Diopsides

Ca-rich pyroxenes have been reported in several EH3 chondrites (Rambaldi et al., 1983; Grossman et al., 1985; Kitamura et al., 1987), but they are generally rare and quite small. We measured seven separate diopsidic to fassaitic grains from Sahara 97159 and Qingzhen (Table 1). REE concentrations are listed in Table 4 and the patterns are shown in Figure 5. Five of the seven diopsides (97-29, 97-53, 97-58, 97-59, and 204-01) are part of chondrules or chondrule fragments. Diopside 97-46 is an individual grain in the matrix of Sahara 97159, and diopside 97-07 is part of an aggregate of diopside grains surrounded by plagioclase and nepheline. All but one of the diopsides have bow-shaped REE patterns that increase from the LREE to the HREE with negative Eu anomalies (Fig. 5); abundances are about an order of magnitude higher than in EET 90102 diopsides. Diopsides 97-07 and 97-53 also have negative Yb anomalies (Fig. 5a). Diopside 97-29 has HREE abundances that are virtually identical to those of 97-07 (including the negative Yb anomaly), but has distinctly elevated LREE abundances and virtually no Eu anomaly (Fig. 5a). This diopside grain occurs adjacent to a plagioclase in a chondrule fragment. However, the LREE enrichment does not appear to be the result of contamination from plagioclase, because abundances of elements characteristic for plagioclase (e.g., Na, Sr, Ba) fall within the ranges observed for the other diopsides measured here. The REE patterns of these diopsides do not seem to be correlated with the wide variations in major element compositions (e.g., FeO and Al_2O_3; Table 1).

4. DISCUSSION

4.1. Volatility-related Anomalies in Enstatite Meteorites

Enstatite meteorites formed under highly reducing conditions and, therefore, offer the opportunity to learn more about processes taking place in a region of the solar nebula distinct

Table 4. REE concentrations (in ppb) in EH3 diopsides[a].

	Diopside grains						
	S97-07	S97-29	S97-46	S97-53	S97-58	S97-59	Q204-01
Anomaly	−Eu, −Yb	−Eu, −Yb	−Eu	−Eu, −Yb	−Eu	−Eu	−Eu
La	420 ± 30	2820 ± 110	480 ± 40	1960 ± 120	560 ± 40	1300 ± 110	380 ± 30
Ce	1520 ± 100	7920 ± 240	1650 ± 100	6880 ± 330	1970 ± 100	3150 ± 290	1480 ± 110
Pr	320 ± 20	1110 ± 60	250 ± 20	1170 ± 80	250 ± 30	790 ± 70	320 ± 40
Nd	2070 ± 70	5300 ± 130	1560 ± 70	5840 ± 290	1260 ± 50	4180 ± 210	2030 ± 130
Sm	840 ± 70	1310 ± 80	640 ± 50	2390 ± 170	550 ± 50	1470 ± 160	760 ± 90
Eu	34 ± 11	340 ± 20	32 ± 8	220 ± 40	120 ± 10	46 ± 58	13 ± 9
Gd	1700 ± 140	1710 ± 110	960 ± 100	4570 ± 330	880 ± 60	3760 ± 500	1290 ± 170
Tb	400 ± 35	340 ± 20	180 ± 20	820 ± 80	170 ± 20	690 ± 80	270 ± 40
Dy	2410 ± 110	2350 ± 80	1830 ± 80	5050 ± 240	1300 ± 60	4430 ± 270	2690 ± 150
Ho	540 ± 50	470 ± 20	450 ± 40	1180 ± 100	260 ± 20	960 ± 110	450 ± 50
Er	1590 ± 80	1510 ± 60	1540 ± 70	3110 ± 150	830 ± 50	3020 ± 190	1500 ± 100
Tm	250 ± 20	220 ± 20	210 ± 20	460 ± 40	110 ± 10	330 ± 50	170 ± 30
Yb	650 ± 110	760 ± 90	1470 ± 120	2290 ± 280	790 ± 70	2250 ± 330	1330 ± 150
Lu	210 ± 40	230 ± 20	310 ± 30	470 ± 60	130 ± 20	360 ± 70	170 ± 40
Eu/Eu*	0.09	0.69	0.12	0.20	0.51	0.06	0.04
Yb/Yb*	0.42	0.51		0.74			

[a] S refers to analyses from Sahara 97159 and Q refers to analyses from Qingzhen; errors are 1σ standard deviation.

from that in which other, more oxidized, meteorites formed. Studies of oldhamite, the main REE carrier in enstatite chondrites (Larimer and Ganapathy, 1987; Crozaz and Lundberg, 1995) suggest that it plays a role analogous to that of hibonite and perovskite in carbonaceous chondrites (Ireland, 1990). Like these minerals, oldhamite exhibits volatility-fractionated REE patterns that were established by high-temperature transient events in the solar nebula (Crozaz and Lundberg, 1995). Oldhamite REE patterns commonly exhibit positive Eu or positive Yb anomalies, or both (Crozaz and Lundberg, 1995). These anomalies have been observed in all enstatite meteorites (including the aubrites: Floss et al., 1990; Floss and Crozaz, 1993) except EL6s. In the EL6 chondrites, CaS invariably has a flat REE pattern with a negative Eu anomaly (Floss and Crozaz, 1993; Crozaz and Lundberg, 1995). This has been attributed to equilibration with plagioclase, which preferentially incorporates Eu (Floss and Crozaz, 1993), but the pattern is sometimes also found in unequilibrated enstatite chondrites (Crozaz and Lundberg, 1995), where such an origin is unlikely. This is the REE pattern that we found in the single oldhamite grain we analyzed in EET 90102 (Fig. 1).

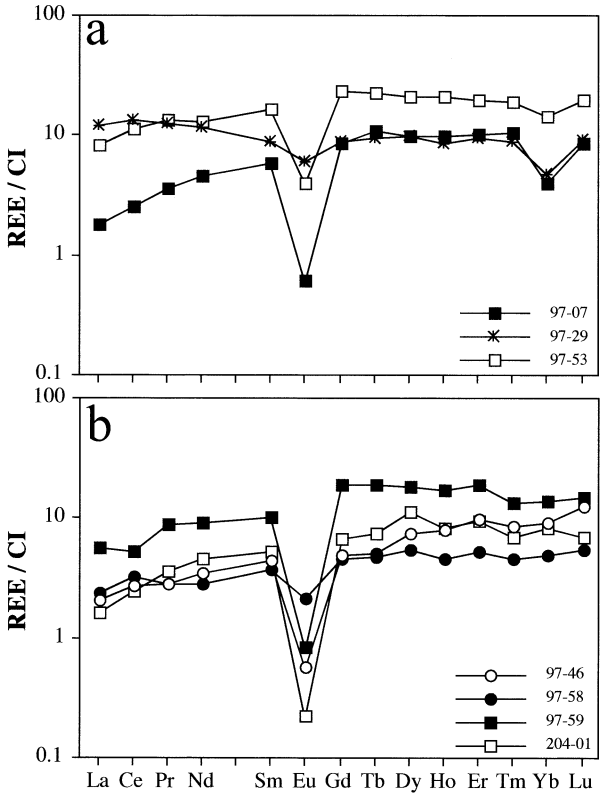

Fig. 5. CI chondrite-normalized REE patterns for diopsides from EH3 chondrites: (a) patterns with Yb anomalies, and (b) patterns without Yb anomalies. The pattern labeled 204-01 is from Qingzhen, the others are from Sahara 97159.

Other minerals in enstatite meteorites also exhibit volatility-related fractionations. REE patterns for enstatite often have negative Sm, Yb, or Eu anomalies in E3, E4, and E5 chondrites (Hsu and Crozaz, 1998). However, in E6 chondrites and aubrites, enstatite only exhibits negative Eu anomalies (Floss and Crozaz, 1993; Crozaz and Lundberg, 1995; Hsu and Crozaz, 1998). The enstatite we measured in EET 90102 contains no anomalies, other than an implied negative Eu anomaly (Table 2; Fig. 2). Plagioclase also exhibits negative Sm anomalies in E3 and E4 chondrites (MacPherson et al., 1996; Hsu, 1998), but again this has not been observed in E6 chondrites or aubrites. In our single analysis of albite from EET 90102, the negative slope of the LREE pattern is so steep (Table 2; Fig. 2) that no information about the Sm concentration could be obtained.

Before this work, the only measurements of diopside in enstatite meteorites have been from aubrites. Although the patterns observed are variable (Floss and Crozaz, 1993; Hsu, 1998), no anomalies other than negative Eu anomalies were found. Thus, we report here the first observation of Yb anom-

alies in diopside from enstatite chondrites. Three of the diopside grains we measured from the EH3 Sahara 97159 have negative Yb anomalies, accompanied by negative Eu anomalies (albeit a small one for diopside 97-29; Fig. 5a). In contrast, the Yb anomalies observed in diopside from EET 90102 are all positive and the two diopsides which have negative Eu anomalies (#2 and #6) do not have Yb anomalies (Fig. 3). There is a slight suggestion that some of the diopsides from EET 90102 have negative Sm anomalies; however, the errors on the values are large and the observed depletions may not be significant. Although errors on the Sm values from relict chondrule fragments are also large, as noted above, consistently low count rates for Sm indicate that the negative Sm anomalies observed in chondrule fragments #2, #3, and #7 (Fig. 4) are probably real (see "Results").

Larimer and Bartholomay (1979) first noted that condensation under reducing conditions produces a new sequence of refractory minerals, many of which are unique to enstatite meteorites. At C/O ratios $\geq$ 1 oldhamite is the first REE-bearing mineral to condense. Lodders and Fegley (1993) carried out REE condensation calculations under the reducing conditions relevant to the formation of enstatite meteorites and found that Eu and Yb are significantly more volatile than other REE and, therefore, might be expected to exhibit volatility-related depletions in oldhamite. The presence of positive rather than the expected negative Eu and Yb anomalies in oldhamite was explained by Lodders and Fegley (1993) by mixing gas and grains from different nebular reservoirs. After condensation of the more refractory REE, the Yb or Yb and Eu remaining in the gas (in a separate nebular reservoir) would condense onto oldhamite grains with flat REE patterns. This model is analogous to that suggested by Grossman (1980) for the formation of group VI patterns in Ca-A1-rich inclusions (CAIs). However, although the scenario outlined is theoretically possible, it would be odd for this to be the dominant process by which oldhamite REE patterns were produced. Furthermore, it is unusual that among the many CaS grains that have been measured in enstatite meteorites (Floss and Crozaz, 1993; Crozaz and Lundberg, 1995), none exhibit the depletions of Eu and Yb predicted by Lodders and Fegley (1993). A sampling of the oldhamite population should show a significant number of REE patterns with negative Eu and Yb anomalies, as well as some with positive anomalies. This is, indeed, what is observed in CAIs, where group III inclusions with negative Eu and Yb anomalies are more common than group VI inclusions with positive Eu and Yb anomalies (MacPherson et al., 1988). Although a sampling bias could theoretically account for the discrepancy, it is highly unlikely that this is the case given that REE concentrations have been measured in more than 200 distinct oldhamite grains from unequilibrated (both EH and EL) enstatite chondrites, equilibrated enstatite chondrites, and aubrites (Larimer and Ganapathy, 1987; Floss et al., 1990; Kurat et al., 1992; Floss and Crozaz, 1993; Grossman et al., 1993; Lodders et al., 1993; Wheelock et al., 1994; Crozaz and Lundberg, 1995; McCoy and Dickinson, 2001).

More puzzling is the fact that the less refractory mineral, enstatite, often exhibits depletions, but not excesses, of these more volatile elements (Hsu and Crozaz, 1998). In our measurements of diopside from the EH3 Sahara 97159, we also find that negative but not positive Yb and Eu anomalies are present. Hsu and Crozaz (1998) discussed the complementarity of enstatite and oldhamite REE patterns, but did not find a satisfactory explanation for it. Thus, there appears to be a first-order discrepancy between the condensation calculations and observations from enstatite meteorites. This disparity suggests that a reexamination of condensation calculations under the reducing conditions of enstatite meteorite formation might be useful, to determine if consideration of additional condensing species and other constraints could resolve the discrepancy. However, such detailed calculations are beyond the scope of this study.

Although Eu and Yb are the most volatile REE during condensation under reducing conditions, Lodders and Fegley (1993) noted that Sm and, to a lesser extent, Tm also have somewhat greater volatilities than the other REE (see their Fig. 2). Again, clear evidence of Sm or Tm anomalies in oldhamite has not been observed, but Sm depletions have been found in enstatite and plagioclase from unequilibrated enstatite chondrites (MacPherson et al., 1996; Hsu and Crozaz, 1998; Hsu, 1998). Here we report, for the first time, the probable presence of negative Sm anomalies in silicates from an equilibrated enstatite chondrite, EET 90102. The Sm depletions seen in the chondrule fragments of EET 90102 (Fig. 4) are, with the exception of a negative Yb anomaly in chondrule #7, not accompanied by negative Eu or Yb anomalies. Such associations, however, are predicted from condensation calculations, because both Eu and Yb are more volatile than Sm (Lodders and Fegley, 1993), and are observed in silicates from unequilibrated enstatite chondrites (MacPherson et al., 1996; Hsu and Crozaz, 1998). The absence of negative Eu anomalies in the chondrule REE patterns may be attributed to the presence of albite, which is enriched in Eu, in the volume measured by the ion microprobe. Indeed, several of the chondrules have distinct positive Eu anomalies (Fig. 4). However, the lack of Yb anomalies is more difficult to understand. One possibility is that they may be masked by the presence of diopside in the analyses.

One analysis of diopside in EET 90102 appears to have a negative Tm anomaly. This is diopside #5 (Fig. 3) with a Tm/Tm* value of 0.44. However, because this is a single occurrence, we prefer to wait for additional confirmation of the existence of Tm anomalies before ascribing any significance to their possible presence in EET 90102. Nevertheless, it is noteworthy that, just as negative anomalies of Yb and Eu are observed in enstatite, but only positive anomalies have been found in oldhamite (Crozaz and Lundberg, 1995; Hsu and Crozaz, 1998), depletions of Sm and (possibly?) Tm are found in the less refractory silicates of enstatite meteorites, but not in the more refractory oldhamite.

4.2. REE Compositions of Chondrule Fragments in EET 90102

EET 90102 contains numerous relict chondrule fragments, which exhibit a variety of REE patterns. Because the chondrule assemblages have not completely recrystallized during metamorphism, their trace element compositions may not be fully equilibrated with the rest of the meteorite. However, they are too fine-grained to allow analysis of their individual minerals. This raises the possibility that there are components in the chondrules that we did not sample in our individual mineral

Table 5. Mineral mixtures used to reproduce EET 90102 chondrule REE compositions.

	Mineral mixtures					Na[b]	Mg[b] (wt.%)	Ca[b]
	albite	diopside #2	diopside #4	oldhamite[a]	enstatite			
chondrule #1	6%	15.5%		0.5%	78%	1.1	13.3	3.0
chondrule #2	1%		3%	0.02%	96%	0.09	17.5	0.58
chondrule #3	6%	4%			90%	0.60	16.4	0.50
chondrule #4	11.6%			0.4%	88%	1.6	12.5	0.73
chondrule #5	15%	10.4%		0.6%	74%	2.1	10.7	1.9
chondrule #6	8%	1%		0.05%	91%	0.75	15.5	0.58
chondrule #7	1%		2%		97%	0.11	16.9	0.33
chondrule #8	28%	2%			70%	3.2	8.0	1.1

[a] REE abundances are based on the pattern in Fig. 1 with concentrations scaled to 50–80 × CI.
[b] Secondary ion mass spectrometry data are not calibrated for matrix effects; see text for more details.

analyses. To test this possibility, we have carried out mixing calculations to try to duplicate the REE compositions measured in the chondrules, using the REE patterns of the minerals we measured in EET 90102. Discrepancies between calculated and measured chondrule REE concentrations could signal the existence of a component not individually analyzed. The calculations were carried out using the REE concentrations of the silicates listed in Table 2 and oldhamite REE concentrations based on the pattern shown in Figure 1, scaled to typical values of 40–80 × CI (see "Results").

The results of the mixing calculations are shown as solid lines in Figure 4, where they are compared to the measured REE patterns. Table 5 lists the proportions of the minerals used to reproduce the REE pattern of each chondrule fragment, as well as the abundances of several major elements measured along with the trace elements during the ion microprobe analyses of the chondrule fragments. These concentrations are not quantitative values because matrix effects from the various phases involved preclude an accurate determination of ion yields for the different elements. They are, however, qualitatively diagnostic of the different minerals that may have been sampled during the measurements.

As is suggested by petrographic observations, the REE compositions of the chondrules are dominated by an enstatite component (Table 5), which accounts for the HREE enrichments observed in many of the patterns (Fig. 4). Lesser amounts of albite and diopside, and minor amounts of oldhamite, contribute to the chondrule patterns. The amount of albite largely reflects Eu concentrations, whereas the amount of oldhamite is determined primarily by the overall REE abundances of the chondrule fragments. The major element compositions of the chondrule analyses are generally consistent with the mineral proportions used to calculate their REE compositions (Table 5). Sodium abundances are highest in those chondrules modeled with large amounts of albite. Similarly, Mg abundances seem to track fairly well the amounts of enstatite used in the modeling, and Ca contents are highest in those chondrules with the largest amounts of oldhamite and diopside.

Despite the fact that the REE compositions of the chondrules can largely be reproduced using the REE patterns of the minerals we analyzed in EET 90102, in detail there are some discrepancies. These nonconformities suggest that at least some chondrules contain components with REE compositions that we have not sampled in our mineral analyses. In particular, we note the presence of a negative Yb anomaly in the REE pattern of chondrule #7 that is not duplicated in the calculated REE composition. Indeed the anomaly cannot be duplicated because none of the mineral phases analyzed in EET 90102 contains a negative Yb anomaly. This chondrule is dominated by enstatite (Fig. 4; Table 5), suggesting that some enstatite in EET 90102 may contain negative Yb anomalies, although we did not sample such grains in our enstatite measurements. The fact that enstatite from other enstatite meteorites commonly exhibits negative Yb anomalies (Hsu and Crozaz, 1998) provides support for this hypothesis. Furthermore, these negative Yb anomalies may be accompanied by negative Sm anomalies (Hsu and Crozaz, 1998), which could account for the Sm depletion observed in chondrule #7.

4.3. The Origin of Diopside in EET 90102

The presence of stable metamorphic diopside in EET 90102 is unique to this meteorite. Fogel (1997a) noted that diopside in EET 90102 is stable because its bulk composition lies either in the enstatite–diopside–oldhamite–alabandite or diopside–alabandite–enstatite stability fields, whereas other E6 chondrites have bulk compositions that lie in the enstatite–oldhamite–alabandite stability field. Furthermore, the diopside stability fields are limited by low oxygen fugacity under conditions of high sulfur fugacity (e.g., the Fe-FeS buffer). The stability of diopside relative to oldhamite can be described by the exchange reaction:

$$CaS_{(oldhamite)} + Mg_2Si_2O_{6(enstatite)} = CaMgSi_2O_{6(diopside)} + MgS_{(in\ alabandite)}$$

We have noted above that some diopside grains in EET 90102 have features, such as the positive Yb anomalies, that have only been observed in oldhamite. Diopside has been reported from an EL3 chondrite (Lin et al., 1991), but no REE compositions have been determined. However, diopside grains from the EH3s analyzed here exhibit negative rather than positive Yb anomalies. Thus, if EET 90102 diopsides were to have evolved from those known to occur in unequilibrated enstatite chondrites, they might be required, at least in some instances, to form positive Yb anomalies from diopsides with negative Yb (and Eu) anomalies. There is no obvious mechanism for such a process.

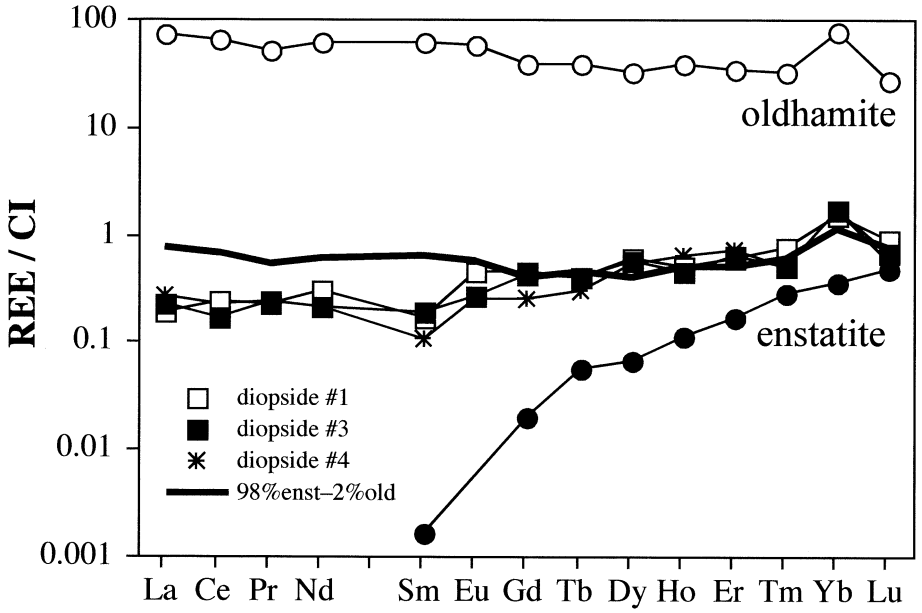

Fig. 6. CI chondrite-normalized REE patterns for enstatite and diopsides #1, #3, and #4 from EET 90102, and oldhamite from Qingzhen (grain Qing2,1Old5.1; data from Crozaz and Lundberg, 1995, scaled to account for new oldhamite sensitivity factors). The solid line shows the results of mixing 2% oldhamite with 98% enstatite.

These observations suggest that diopside in EET 90102 may have formed during metamorphic reequilibration from enstatite and oldhamite, via a reaction like the one noted above, and inherited its REE characteristics from these minerals. Lodders et al. (1993) suggested a similar origin for the diversity of REE patterns in aubritic diopside, although the detailed reaction to produce diopside in the aubrites differs from the one discussed here.

We can test this hypothesis by attempting to reproduce the REE patterns of the diopsides with positive Yb anomalies. Oldhamite grains with positive Yb anomalies are common in unequilibrated enstatite chondrites (Crozaz and Lundberg, 1995). Three distinct patterns are observed. In two of these (types C and D), positive Eu anomalies accompany the Yb anomalies; however, pattern B is relatively flat with only a positive Yb anomaly (see Crozaz and Lundberg, 1995 for a discussion of oldhamite REE patterns). Figure 6 compares diopsides #1, #3, and #4 from EET 90102 with the results of mixing 2% oldhamite with a type B pattern with 98% enstatite from EET 90102. The oldhamite grain used for this calculation is Qing2,1Old5.1 (see Table 2 of Crozaz and Lundberg, 1995). Although this oldhamite grain comes from an EH3 chondrite, the type B pattern has also been observed in oldhamite from the EL3 chondrites (Crozaz and Lundberg, 1995). REE abundances of the oldhamite were adjusted to take into account new sensitivity factors for CaS (Fahey et al., 1995). Absolute concentrations are, therefore, ~40% lower than those reported by Crozaz and Lundberg (1995). However, the shape of the pattern is not affected.

The compositions of the diopside grains are reproduced quite well for the HREE, including the positive Yb anomaly (Fig. 6). The agreement is not so good for the LREE. One possible reason for the discrepancy is that it may be due to a partitioning effect. In general, the smaller HREE are more easily accommodated into the pyroxene structure (where they substitute for Ca in the M2 sites) than the larger LREE (McKay, 1989). Thus, there may have been preferential discrimination against the LREE during metamorphic formation of diopside, an effect which is obviously not accounted for in these mixing calculations. Alternative explanations include the possibility that the oldhamite from which these diopsides formed is more LREE-depleted than those measured by Crozaz and Lundberg (1995), and the possibility of redistribution of some of the LREE into surrounding phases (e.g., plagioclase) during metamorphism.

Nevertheless, the Yb anomalies observed in diopside from EET 90102 can clearly be explained by their derivation from oldhamite during the metamorphic formation of this phase. Other diopside REE patterns may derive more directly from enstatite. Fogel (1997a) has noted that enstatite CaO contents in equilibrated enstatite chondrites (including EET 90102) lie close to the enstatite–diopside phase boundary and, thus, should result in the formation of stable diopside during metamorphic equilibration. The REE patterns of diopsides #2, #5, and #6 are qualitatively similar to type II enstatite REE patterns of unequilibrated enstatite chondrites (Hsu and Crozaz, 1998) in their slopes and overall REE abundances, although they do not exhibit the negative Sm and Yb anomalies sometimes observed in the enstatites. Thus, some of the diopsides in EET 90102 may have formed largely from enstatite with similar REE compositions during metamorphism. If the slight Sm depletions noted in some of the diopside grains are indeed real, this would also be consistent with the presence of a significant enstatite component in the diopside REE compositions. Indeed, we noted earlier the presence of negative Sm anomalies in some of the enstatite-dominated chondrule fragments.

4.4. Thermal History of EET 90102

The presence of Sm and Yb anomalies in EET 90102 is unusual for EL6 chondrites. As we noted above, oldhamite and enstatite from unequilibrated enstatite meteorites display a variety of patterns with various anomalies. In this study we also report the first analyses of diopside with volatility-related fractionations from unequilibrated enstatite chondrites. In EL6 chondrites, however, the same phases display no anomalies (except for negative Eu anomalies). Even oldhamite, which exhibits Yb anomalies in both aubrites (Floss and Crozaz, 1993) and unequilibrated enstatite chondrites (Crozaz and Lundberg, 1995) only has a flat REE pattern with a negative Eu anomaly in EL6 chondrites (Floss and Crozaz, 1993; Crozaz and Lundberg, 1995), similar to the CaS grain measured here (Fig. 1). Floss and Crozaz (1993) attributed this EL6 oldhamite pattern to the prolonged thermal metamorphism experienced by these meteorites, during which the REE equilibrated with surrounding phases. The major and minor element chemistry of EET 90102 suggest that it is well equilibrated (Fogel, 1997a). Yet we have here, for the first time, an EL6 chondrite that contains anomalies in both Yb and Sm. Furthermore, although diopside REE patterns are generally similar in shape and overall abundance levels, they do exhibit heterogeneity with regard to the presence or absence of Yb and Eu anomalies. This suggests that there may be something different about either the trace element starting composition or the thermal history (or both) of EET 90102 from other EL6 chondrites.

We can compare the REE compositions of the EET 90102 minerals with those observed in other enstatite meteorites to draw conclusions about the distinctiveness of trace element compositions in EET 90102. We noted earlier that the REE pattern for EET 90102 enstatite is similar to pattern III of Hsu and Crozaz (1998). This pattern is found in all types of enstatite meteorites, including aubrites. Furthermore, there is indirect evidence from the REE patterns of the chondrule fragments (see above) that some enstatite in EET 90102 may have negative Sm or Yb anomalies, or both, like those observed in other enstatite meteorites (Hsu and Crozaz, 1998). Similarly, the REE pattern for albite from EET 90102 is typical of that observed for plagioclase from enstatite meteorites (Floss and Crozaz, 1993; Hsu, 1998). A comparison of oldhamite patterns is hampered by the fact that we were only able to analyze one CaS grain from EET 90102. However, as we have mentioned before, its REE pattern is like those observed in other EL6s and is one of the most common patterns seen in the enstatite meteorite group (Floss and Crozaz, 1993; Crozaz and Lundberg, 1995). The REE patterns of EET 90102 diopside (Fig. 3) are generally not similar to those that we measured in the EH3 chondrites (Fig. 5). However, we have argued above that diopside in EET 90102 probably formed through metamorphic equilibration of enstatite and oldhamite and inherited its REE patterns from these precursor materials, which do exhibit patterns previously observed in enstatite meteorites. Thus, there is no compelling evidence that the trace element compositions of EET 90102 are unique to this meteorite.

Using the enstatite–oldhamite geothermometer developed by Larimer and Buseck (1974), Fogel et al. (1989) found that most EL6 chondrites have been metamorphosed to temperatures exceeding 900 to 1000 °C. Wasson et al. (1994) obtained a similar estimate of ~950°C based on the equilibrium between ferrosilite in enstatite and Si-bearing kamacite. Furthermore, EL6 alabandite compositions indicate equilibration temperatures of 200 to 500 °C (Skinner and Luce, 1971; Fogel, 1997a), implying that cooling rates from peak temperatures were slow. Additional evidence for slow cooling includes low P contents in kamacite and the presence of schreibersite in these meteorites (Fogel, 1997a). Thus, most EL6 chondrites appear to have experienced slow cooling from temperatures near 1000°C to 200 to 500 °C. In contrast, EET 90102 appears to have been quenched from a high metamorphic temperature (~900°C). Applying the two-pyroxene geothermometer of Lindsley et al. (1981) to the enstatite and diopside of EET 90102 yields an average minimum metamorphic temperature of 890°C (Fogel, 1997a). Very similar temperatures are recorded by the FeS and CaS contents of alabandite (875°C and 900°C), indicating that cooling was rapid enough to "lock in" these high temperatures in the sulfides. In addition, Fogel (1997a) noted that EET 90102 does not contain schreibersite commonly found in other EL6s and has high P contents in the metal, indicating that its minimum temperature of equilibration must have been higher than the 800°C required to precipitate schreibersite (Kubaschewski, 1982).

In addition to the thermometric evidence presented above, the presence of abundant relict chondrule fragments in EET 90102 suggests that it may be less thermally metamorphosed than some other EL6 chondrites. Although chondrule textures are recognized in some EL6s like Yilmia and Hvittis (Buseck and Holdsworth, 1972; Rubin, 1983), most studies have noted that visible chondrules are not observed in the equilibrated enstatite chondrites (Keil and Anderson, 1965; Mason, 1966; Keil, 1968, Rubin, 1984). Thus, the data seem to indicate that EET 90102 experienced a different thermal history from most EL6 chondrites. Although it reached the same high metamorphic temperatures as other EL6s, it does not seem to have undergone the long slow cooling that they apparently did. It is likely that the variability observed in the diopside REE patterns (e.g., the presence or absence of Yb anomalies) can be attributed to this rapid cooling, as REE compositions may not have had time to completely homogenize in diopside after its metamorphic formation. The presence of Sm and Yb anomalies in other phases of EET 90102 may also be due to its less equilibrated nature. Alternatively, it is also possible that this is simply the result of inadequate sampling. Extensive trace element measurements of other EL6 chondrites could reveal the presence of various anomalies in the silicates of these meteorites, as well.

4.5. The Significance of Diopside in EET 90102

As we have noted above, EET 90102 is the first EL6 chondrite found to contain diopside. Fogel (1997a) pointed out that its discovery is of significance for the understanding enstatite meteorite petrogenesis. Although the three enstatite meteorite groups may represent separate parent bodies (Keil, 1989, but see Fogel, 1997b), it is generally acknowledged that the achondritic aubrites must have formed from an enstatite chondrite-like precursor. However, the disparity in diopside abundances between aubrites and enstatite chondrites has been difficult to reconcile. In one attempt to do so, Fogel et al. (1988) suggested

that diopside in the aubrites could have formed by the oxidation of oldhamite. However, the viability of this process is limited because the quantity of oldhamite present in the enstatite chondrites is insufficient to account for the large amount of diopside present in some aubrites (e.g., up to 20% in Norton County). In addition, although a variety of REE patterns have been observed in aubritic diopside (Floss and Crozaz, 1993; Hsu, 1998), these patterns do not provide compelling evidence for its formation from oldhamite. Some patterns are bow-shaped with negative Eu anomalies, consistent with what is expected from igneous partitioning constraints, whereas others are flat to slightly LREE-enriched with little or no Eu anomalies. However, it has been suggested that the presence of tiny melt inclusions within the grains largely accounts for these latter patterns (Hsu, 1998). No patterns have been observed in aubritic diopside that display the positive Eu and Yb anomalies commonly found in oldhamite.

The presence of diopside-bearing enstatite chondrites may simplify aubrite formation by providing an alternative method for producing the abundant diopside present in the aubrites, through the melting of a diopside-bearing enstatite chondrite protolith. Fogel (1997a) pointed out that, under equilibrium melting conditions, diopside would be consumed early during the melting of enstatite chondrites with bulk compositions similar to those of EET 90102. Removal of these melts from the source provides a melt that would produce diopside during equilibrium crystallization. Even small amounts of diopside in the source could provide significant amounts of diopside, if the melt is drawn off early. Thus, diopside abundances in aubrites could be reproduced by varying the degree of melting and the stages at which melt is removed from the source region. This process would be consistent with the argument of Hsu (1998) who suggested that trace element data and petrographic observations indicate that diopside in aubrites formed by igneous crystallization.

5. CONCLUSIONS

Silicates in EET 90102 have REE patterns with anomalies indicative of formation under highly reducing conditions. Such anomalies have not been observed in other EL6s, although they are known from unequilibrated enstatite chondrites. Diopside REE patterns in EET 90102 differ from those measured in diopside from the EH3 chondrites Qingzhen and Sahara 97159. Some EET 90102 diopsides exhibit anomalies that are known only from oldhamite REE patterns, suggesting that they inherited their REE characteristics from CaS during metamorphic formation of diopside from enstatite and oldhamite. Other grains have REE patterns that do not exhibit such anomalies and may primarily reflect the role of enstatite in the formation of metamorphic diopside. EET 90102 appears to have been quenched from high metamorphic temperatures (Fogel, 1997a) and, thus, there may not have been time to completely homogenize REE compositions in EET 90102 diopside after its formation.

Acknowledgments—Constructive reviews by G. Crozaz, K. Keil, and two anonymous reviewers provided significant improvements to this manuscript and are greatly appreciated. This work was supported by NSF grant EAR99-80394 (G. Crozaz, P.I.) and NASA grants NAG5-4838 and NAG5-10505 (R. A. Fogel, P.I.).

Associate editor: H. Palme

REFERENCES

Alexander C. M. O. D. (1994) Trace element distributions within ordinary chondrite chondrules: Implications for chondrule formation conditions and precursors. *Geochim. Cosmochim. Acta* **58,** 3451–3467.

Anders E. and Grevesse N. (1989) Abundances of the elements: Meteoritic and solar. *Geochim. Cosmochim. Acta* **53,** 197–214.

Buseck P. R. and Holdsworth E. F. (1972) Mineralogy and petrology of the Yilmia enstatite chondrite. *Meteoritics* **7,** 429–447.

Crozaz G. and Lundberg L. L. (1995) The origin of oldhamite in unequilibrated enstatite chondrites. *Geochim. Cosmochim. Acta* **59,** 3817–3831.

Fahey A., Huss G., Wasserburg G., and Lodders K. (1995) REE abundances and Cr isotopic composition of oldhamite and associated minerals from the Peña Blanca Spring aubrite. *Lunar Planet. Sci. XXVI*. Lunar Planet. Inst., Houston., 385–386. (abstr.).

Floss C. and Crozaz G. (1993) Heterogeneous REE patterns in oldhamite from the aubrites: Their nature and origin. *Geochim. Cosmochim. Acta* **57,** 4039–4057.

Floss C. and Jolliff B. (1998) Rare earth element sensitivity factors in calcic plagioclase (anorthite). In *Secondary Ion Mass Spectrometry, SIMS XI* (eds. G. Gillen, R. Lareau, J. Bennett, and F. Stevie), pp. 785-788. John Wiley & Sons.

Floss C., and Fogel R. A. (2001) Diopside-bearing EL6 EET 90102: Insights from rare earth element distributions. *Lunar Planet. Sci. XXXII*. Lunar Planet. Inst., Houston. #1623. (abstr.).

Floss C., Strait M. M., and Crozaz G. (1990) Rare earth elements and the petrogenesis of aubrites. *Geochim. Cosmochim. Acta* **54,** 3553–3558.

Floss C., Lin Y., Kimura M., and Fogel R. A. (2001) Heterogeneous REE patterns in diopside from EL6 chondrite EET 90102. *Met. Planet. Sci.* **36,** A59 (abstr.).

Fogel R. A. (1995) Diopside in equilibrated enstatite chondrites: EET90102—the first diopside bearing EL6 chondrite. *Lunar Planet. Sci. XXVI*, 411–412. Lunar Planet. Inst., Houston. (abstr.).

Fogel R. A. (1997a) On the significance of diopside and oldhamite in enstatite chondrites and aubrites. *Met. Planet. Sci.* **32,** 577–591.

Fogel R. A. (1997b) The enstatite chondrite-achondrite link reforged: Solution of the titanium in troilite problem. *Met. Planet. Sci.* **32,** A43 (abstr.).

Fogel R. A., Hess P. C., and Rutherford M. J. (1988) The enstatite chondrite-achondrite link. *Lunar Planet. Sci. XIX*, 342–343. Lunar Planet. Inst., Houston (abstr.).

Fogel R. A., Hess P. C., and Rutherford M. J. (1989) Intensive parameters of enstatite chondrite metamorphism. *Geochim. Cosmochim. Acta* **53,** 2735–2746.

Grossman L. (1980) Refractory inclusions in the Allende meteorite. *Ann. Rev. Earth Planet. Sci.* **8,** 559–608.

Grossman J. N., Rubin A. E., Rambaldi E. R., Rajan R. S., and Wasson J. T. (1985) Chondrules in the Qingzhen type-3 enstatite chondrite: Possible precursor components and comparison to ordinary chondrite chondrules. *Geochim. Cosmochim. Acta* **49,** 1781–1795.

Grossman J. N., MacPherson G. J., and Crozaz G. (1993) LEW 87223: A unique E chondrite with possible links to H chondrites. *Meteoritics* **28,** 358.

Hsu W. (1995) Ion microprobe studies of the petrogenesis of enstatite chondrites and eucrites. Ph.D. thesis, Washington University.

Hsu W. (1998) Geochemical and petrographic studies of oldhamite, diopside, and roedderite in enstatite meteorites. *Met. Planet. Sci.* **33,** 291–301.

Hsu W. and Crozaz G. (1998) Mineral chemistry and the origin of enstatite in unequilibrated enstatite chondrites. *Geochim. Cosmochim. Acta* **62,** 1993–2004.

Ireland T. R. (1990) Presolar isotopic and chemical signatures in hibonite-bearing refractory inclusions from the Murchison carbonaceous chondrite. *Geochim. Cosmochim. Acta* **54,** 3219–3237.

Keil K. (1968) Mineralogical and chemical relationships among enstatite chondrites. *J. Geophys. Res.* **73,** 6945–6976.

Keil K. (1989) Enstatite meteorites and their parent bodies. *Meteoritics* **24,** 195–208.

Keil K. and Anderson C. A. (1965) Electron microprobe study of the Jajh deh Kot Lalu enstatite chondrite. *Geochim. Cosmochim. Acta* **29,** 621–632.

Kimura M., Lin Y., and Hiyagon H. (2000) Unusually abundant refractory inclusions and iron-oxide-rich silicates in an EH3 chondrite, Sahara 97159. *Met. Planet. Sci.* **35,** A87 (abstr.).

Kitamura M., Watanabe S., Isobe H., and Morimoto N. (1987) Diopside in chondrules of Yamato-691 (EH3). *Mem. Natl. Inst. Polar Res. (Spec. Issue)* **46,** 113–122.

Kubaschewski O. (1982) *Iron Binary Phase Diagrams*. Springer-Verlag. 185 pp.

Kurat G., Zinner E., and Brandstätter F. (1992) An ion microprobe study of an unique oldhamite-pyroxenite fragment from the Bustee aubrite. *Meteoritics* **27,** 246–247.

Larimer J. W. and Buseck P. R. (1974) Equilibration temperatures in enstatite chondrites. *Geochim. Cosmochim. Acta* **38,** 471–477.

Larimer J. W. and Bartholomay M. (1979) The role of carbon and oxygen in cosmic gases: Some applications to the chemistry and mineralogy of enstatite chondrites. *Geochim. Cosmochim. Acta* **43,** 1455–1466.

Larimer J. W. and Ganapathy R. (1987) The trace element chemistry of CaS in enstatite chondrites and some implications regarding its origin. *Earth Planet. Sci. Lett.* **84,** 123–134.

Lin Y. T., Nagel H.-J., Lundberg L. L., and El Goresy A. (1991) *MAC88136—the first EL3 chondrite. Lunar Planet. Sci. XXII*, 812–814. Lunar Planet. Inst., Houston (abstr.).

Lindsley D. H., Grover J. E., and Davidson P. M. (1981) The thermodynamics of the $Mg_2Si_2O_6$-$CaMgSi_2O_6$ join: A review and an improved model. In *Advances in Physical Geochemistry 1. Thermodynamics of Minerals and Melts* (eds. R. C. Newton, A. Navrotsky, and B. J. Wood), pp. 149-175. Springer-Verlag.

Lodders K. and Fegley B. (1993) Lanthanide and actinide chemistry at high C/O ratios in the solar nebula. *Earth Planet. Sci. Lett.* **117,** 125–145.

Lodders K., Palme H., and Wlotzka F. (1993) Trace elements in mineral separates of the Peña Blanca Spring aubrite: Implication for the evolution of the aubrite parent body. *Meteoritics* **28,** 538–551.

MacPherson G. J., Wark D. A., and Armstrong J. T. (1988) Primitive material surviving in chondrites: Refractory inclusions. In *Meteorites and the Early Solar System* (eds. J. F. Kerridge and M. S. Matthews), pp. 746–807. University of Arizona Press, Tucson.

MacPherson G. J., Zinner E. K., and Grossman J. N. (1996) Plagioclase-rich chondrules in the ungrouped E3 chondrite LEW 87234: Trace elements and a suggestion of excess ^{26}Mg. *Meteoritics* **31,** A81–A82 (abstr.).

Mason B. (1966) The enstatite chondrites. *Geochim. Cosmochim. Acta* **30,** 23–39.

McCoy T. J., and Dickinson T. L. (2001) REE patterns and abundances from sulfides in an oldhamite-rich lithology of the ALH 84008 aubrite. *Lunar Planet. Sci.* XXXII:#1221.

McKay G. A. (1989) Partitioning of rare earth elements between major silicate minerals and basaltic melts. In *Geochemistry and Mineralogy of Rare Earth Elements* (eds. B. R. Lipin and G. A. McKay), pp. 45-77. Mineralogical Society of America.

Okada A., Keil K., and Taylor G. J. (1981) Unusual weathering products of oldhamite parentage in the Norton County enstatite achondrite. *Meteoritics* **16,** 141–152.

Rambaldi E. R., Rajan R. S., Wang D., and Housley R. M. (1983) Evidence for relict grains in chondrules of Qingzhen, an E3 type enstatite chondrite. *Earth Planet. Sci. Lett.* **66,** 11–24.

Rubin A. E. (1983) Impact melt clasts in the Hvittis enstatite chondrite breccia: Implications for a genetic relationship between EL chondrites and aubrites. *Proc. Lunar Planet. Sci. Conf. 14th, J. Geophys. Res.* **88,** B293–B300.

Rubin A. E. (1984) The Blithfield meteorite and the origin of sulfide-rich, metal-poor clasts and inclusions in brecciated enstatite chondrites. *Earth Planet. Sci. Lett.* **67,** 273–283.

Shima M. and Honda M. (1967) Distributions of alkali, alkaline earth and rare earth elements in component minerals of chondrites. *Geochim. Cosmochim. Acta* **31,** 1995–2006.

Skinner B. J. and Luce F. D. (1971) Solid solutions of the type (Ca,Mg,Mn,Fe)S and their use as geothermometers for the enstatite chondrites. *Am. Mineral.* **56,** 1269–1296.

Wasson J. T., Kallemeyn G. W., and Rubin A. E. (1994) Equilibration temperatures of EL chondrites: A major downward revision in the ferrosilite contents of enstatite. *Meteoritics* **29,** 658–662.

Watters T. R., Prinz M. (1979) Aubrites: Their origin and relationship to enstatite chondrites. *Proc. Lunar Planet. Sci. Conf. 10th*, 1073–1093.

Wheelock M. M., Keil K., Floss C., Taylor G. J., and Crozaz G. (1994) REE geochemistry of oldhamite-dominated clasts from the Norton County aubrite: Igneous origin of oldhamite. *Geochim. Cosmochim. Acta* **58,** 449–458.

Zinner E. and Crozaz G. (1986a) A method for the quantitative measurement of rare earth elements in the ion microprobe. *Intl. J. Mass Spec. Ion. Processes* **69,** 17–38.

Zinner E., Crozaz G. (1986b) Ion probe determination of the abundances of all the rare earth elements in single mineral grains. *SIMS V*, 444–446.